Published in final edited form as:
Rep U S. 2014 September ; 2014: 3476–3482. doi:10.1109/IROS.2014.6943047.

Task-Space Motion Planning of MRI-Actuated Catheters for Catheter Ablation of Atrial Fibrillation

Tipakorn Greigarn and **M. Cenk Çavuşoğlu**
Department of Electrical Engineering and Computer Science, Case Western Reserve University, Cleveland, OH

Abstract

This paper presents a motion planning algorithm for Magnetic Resonance Imaging (MRI) actuated catheters for catheter ablation of atrial fibrillation. The MRI-actuated catheters is a new robotic catheter concept which utilizes MRI for remote steering and guidance. Magnetic moments generated by a set of coils wound near the tip are used to steer the catheter under MRI scanner magnetic field. The catheter during an ablation procedure is modeled as a constrained robotic manipulator with flexible joints, and the proposed motion-planning algorithm calculates a sequence of magnetic moments based on the manipulator model to move the tip of the catheter along a predefined trajectory on the surface of the left atrium. The difficulties in motion planning of the catheter are due to kinematic redundancy and underactuation. The proposed motion planning algorithm overcomes the challenges by operating in the task space instead of the configuration space. The catheter is then regulated around this nominal trajectory using feedback control to reduce the effect of uncertainties.

I. Introduction

Catheter ablation of atrial fibrillation has become the standard treatment for atrial fibrillation [1]. The procedure is performed by inserting the catheter from the groin or neck. Then the catheter is navigated to the right atrium where it enters the left atrium through a transseptal puncture. The procedure most commonly aims to electrically isolate pulmonary veins by creating non-conducting lesions around the veins using radio frequency energy [1], [2]. The catheter is often guided using mapping catheters and fluoroscopy [1].

It was pointed in [2] that the success rate of manual ablations appear to increase with skill and experience of the physician. Robotic catheters can improve the efficacy and safety of the procedure by reducing radiation exposure, alleviating physical demand on the physician, improving catheter stability, and increasing reproducibility of the procedure [1], [3]. Two commercially available robotic catheters are Sensei Robotic Navigation System and Niobe Remote-Controlled Magnetic Navigation System. The former is remotely steered by two steerable sheaths which are manipulated using pull-wire mechanism, while the latter uses two external magnets to remotely steer the catheter equipped with a permanent magnet. Mapping catheters such as CARTO-3 are used for navigation in both systems [3].

They can be reached via email at txg92@case.edu and cavusoglu@case.edu respectively.

The catheter ablation procedure is benefited by the introduction of Magnetic Resonance Imaging (MRI), which offers superior soft-tissue visualization without radiation exposure [4]. MRI has been used pre-procedurally to obtain a detailed anatomical information of the pulmonary veins and left atrium, and post-procedurally to detect complications. MRI can also be used to visualize lesions formed by the ablation process [1], [5]. The feasibility of real-time catheter ablation guidance and lesion visualization have also been demonstrated in [4], [5].

Remote-controlled catheters which utilize MRI for remotesteering and guidance are proposed in [6], [7]. The proposed catheters are equipped with a set of orthogonal coils. Magnetic moments generated by the coils deflect the catheter under Magnetic Resonance (MR) magnetic field using Lorentz force. The MRI-actuated catheters present an opportunity to perform mapping, remote-steering, ablation guidance, and lesions visualization, as an integrated solution in MR environment.

The catheter, being a continuum mechanism, has infinite degrees of freedom, which can be modeled using beam theory [8], [9]. To reduce the complexity of the problem such that motion planning is tractable while preserving the characteristics of the system, the continuous body of the catheters is discretized into n-rigid links connected by torsional springs. The model is known as pseudo-rigid-body (PRB) model. A PRB model with three rotational joints is presented in [10].

The motion-planning algorithm presented in this paper calculates a sequence of magnetic moments needed to move the tip of the MRI-actuated catheter along a predefined trajectory on a surface. Motion planning and control of flexible catheters with similar objectives have been studied in [11]–[13]. An evaluation of task space and joint space control of a pull-wire actuated flexible catheter is presented in [11]. Task-space control of interleaved continuum-rigid manipulators is considered in [12]. Jacobian-based control for concentric-tube continuum robots is described in [13]. Motion planning of the MRI-actuated catheter presented here have its own distinct complications due to its unique actuation method. Two main challenges in motion planning considered in this paper are kinematic redundancy and underactuation. Kinematic redundancy arises from the fact that the surface the catheter operates on is two dimensional while the approximated model required relatively higher degrees of freedom to approximate the continuum model. Underactuation is also a consequence of having high degrees of freedom since the torques available to the catheter is constrained to a two-dimensional surface perpendicular to the MR magnetic field.

The planning algorithm avoid such difficulties by performing motion planning in the task space instead of the configuration space. By exploiting the fact that the actuation and the surface has the same dimension, planning problem can be greatly simplified. The algorithm has two components. First, an open-loop planner calculates the magnetic moments such that the desired tip trajectory is obtained in a noise-free environment. Then, a feedback policy is combined with the open-loop plan to mitigate the effect of uncertainties and regulate the catheter around the nominal trajectory.

The remainder of this paper is organized as follows: the modeling of the catheter is formulated in Section II, the motion-planning algorithm is introduced in Section III, the feedback policy is described in Section IV, simulation results are presented in Section V, followed by conclusions in Section VI.

II. Modeling

A. Equations of Motion

The catheter, being a deformable object, has infinite degrees of freedom. To reduce the dimension of the problem such that motion planning can be performed while preserving the characteristics of the system, the continuous body of the catheter is approximated by an *n*-link manipulator. Since the stiffness of the catheter along its axial direction is much higher than the directions perpendicular to it, torsional rotation is neglected and only bending is considered in the approximated model. As a result, each joint has only two degrees of freedom and the *n*-joint model has 2*n* degrees of freedom. The elasticity of the catheter is modeled by a torsional spring at each joint. The catheter and an *n*-link model are shown in Fig. 1. The base of the catheter is assumed to be at the transseptal puncture where the catheter enters the left atrium.

Let $\mathscr{C} \subset \mathbb{R}^{2n}$ be the set of possible joint angles, also called the configuration space, and $\theta \in \mathscr{C}$ be a joint angle vector. The configuration of the catheter's tip is given by,

$$g_{st}(\theta)=e^{(\hat{\xi}_1\theta_1+\hat{\xi}_2\theta_2)}\dots e^{(\hat{\xi}_{2n-1}\theta_{2n-1}+\hat{\xi}_{2n}\theta_{2n})}g_{st}(0), \quad (1)$$

where $g_{st}:\mathscr{C} \to SE(3)$ maps joint angles into tip configurations, $\hat{\xi}_i \in se(3)$ are the joint twists, and $g_{st}(0) \in SE(3)$ is the initial configuration of the catheter's tip with respect to the spatial frame. The spherical joint rotations are described by linear combinations of twists in (1) to avoid assuming order of rotation.

When performing ablation, the catheter's tip has to be in contact with the surface of the left atrium. The contact can be described by an equality constraint, denoted by $h(\theta) = 0$. For example, the constraint for a flat surface is given by

$$h(\theta)=(p(\theta)-p_0)^T n_0,$$

where $p(\theta)$ is the position of the catheter's tip, p_0 is the point that the surface passes through, and n_0 is the vector orthogonal to the surface. The constraint is referred to as the tip constraint in this paper and it can be defined similarly for other surfaces.

Equations of motion of the constrained manipulator can be derived using Lagrange's equation's together with the contraint $h(\theta) = 0$. The equations of motion has the following form,

$$M(\theta)\ddot{\theta}+C(\theta,\dot{\theta})\dot{\theta}+N(\theta)+\nabla h(\theta)\lambda=\tau, \quad (2)$$

where $M(\theta) \in \mathbb{R}^{2n\times 2n}$ is the manipulator inertia matrix, $C(\theta,\dot{\theta}) \in \mathbb{R}^{2n\times 2n}$ is the sum of the Coriolis matrix and a viscous damping coefficient matrix, $N(\theta) \in \mathbb{R}^{2n}$ is the conservative forces due to the joint springs, and $\tau \in \mathbb{R}^{2n}$ are the joint torques. The constraint force, $\nabla h(\theta)\lambda \in \mathbb{R}^{2n}$, are the forces exerted by the surface to keep the joint angles on the constraint surface. The columns of $\nabla h(\theta) \in \mathbb{R}^{2n}$ form a basis for the constraint forces while $\lambda \in \mathbb{R}$ specifies the relative magnitude of the forces [14]. Because each spherical joint rotation is described by the sum of twists as in (1), $N(\theta) = K\theta$, where $K \in \mathbb{R}^{2n\times 2n}$ is a spring stiffness coefficient matrix.

Generally, during catheter ablation, the catheter moves with low velocity and acceleration. Hence, the inertial and Coriolis forces are negligible, and (2) is reduced to

$$C(\theta,\dot{\theta})+K\theta+\nabla h(\theta)\lambda=\tau, \quad (3)$$

where $C(\theta)$ now contains only the viscous damping coefficient matrix.

The constraint forces of the reduced system described by (3) can be calculated as follows. Since, the constraint forces are orthogonal to the constraint surface, they produce no work, and $\nabla h(\theta)^T\dot{\theta}=0$ [14]. Using this fact and (3), λ can be calculated from

$$\lambda=(\nabla h^T C^{-1}\nabla h)^{-1}\nabla h^T C^{-1}(-K\theta+\tau).$$

B. Joint Torques and Actuation

The joint torque vector in (3) is a combination of several terms. The joint torques created by the magnetic moments from the coils, $u \in \mathbb{R}^3$, are denote by $\tau_u \in \mathbb{R}^{2n}$. Similarly, the disturbance forces, denoted by $w \in \mathbb{R}^3$, give rise to the disturbance joint torques, denoted by $\tau_w \in \mathbb{R}^{2n}$. Friction between the tip and the surface is denoted by $f_\mu \in \mathbb{R}^2$, and the joint torques associated with it are denoted by $\tau_\mu \in \mathbb{R}^{2n}$. The total joint torques can then be written as the sum of the three torques given by

$$\tau=\tau_u+\tau_w+\tau_\mu. \quad (4)$$

The actuation torques are produced by the cross product of the MRI scanner magnetic field and the catheter's magnetic moment. The joint torques from the actuation can be calculated from the product of the manipulator Jacobian, denoted by J_{su}^b, and a wrench containing the cross product between the magnetic moment and the magnetic field in its rotational component [14],

$$\tau_u={J_{su}^b}^T(\theta)\begin{bmatrix} 0_{3\times 1} \\ u \times b \end{bmatrix}, \quad (5)$$

where $b \in \mathbb{R}^3$ denotes the magnetic field and the magnetic moment u is considered the input of the system. Note that τ_u is linear in u because the cross product is a linear operator.

Moreover, the degrees of freedom of the actuation is reduced to two because of the cross product. The disturbance joint torques can be calculated similarly from

$$\tau_w = {J_{sw}^b}^T(\theta) \begin{bmatrix} w \\ 0_{3\times 1} \end{bmatrix}.$$

Coulomb friction is used to model the friction between the catheter's tip and the surface. The set of all contact forces, $f_c \in \mathbb{R}^3$, that cause no slippage between the tip and the surface form a *friction cone* [14], which is given by

$$FC = \{f_c \in \mathbb{R}^3 \colon \sqrt{f_{c1}^2 + f_{c2}^2} \le \mu f_{c3}\},$$

where μ is the Coulomb friction coefficient, and the coordinate frame of f_c is aligned with the z-axis pointing in the direction of the inward surface normal. Friction is calculated from the contact forces as

$$f_\mu = \begin{cases} -[f_{c1} \quad f_{c2}]^T, & \text{if } f_c \in FC \\ -\mu |f_{c3}| \frac{\dot{x}}{\|\dot{x}\|}, & \text{if } f_c \notin FC \end{cases}$$

Where $\dot{x} \in \mathbb{R}^2$, a function of $\dot{\theta}$, is the tip velocity on the surface. The joint torques caused by friction are calculated as

$$\tau_\mu = {J_{s\mu}^s}^T(\theta) f_\mu.$$

III. Task-Space Motion Planning

In this section, the motion-planning algorithm that calculates the control input trajectory that moves the tip of the catheter along a reference trajectory on the surface is presented.

The task space is defined as the surface of the left atrium. Since the degree of freedom of the catheter is higher than the dimension of the task space and the actuation, even in the approximated model studied here, the catheter is said to be both redundant and underactuated. As a result, the solutions of the inverse kinematics are not unique due to kinematic redundancy. On the other hand, only some of the configurations are reachable because of underactuation. To circumvent the difficulties, planning is carried out in the task space instead of the configuration space.

To perform motion planning in the task space, a description of the system in the space must first be obtained. A derivation of the equations of motion in the task space is given in Section III-A, followed by the motion-planning algorithm in Section III-B.

NIH-PA Author Manuscript

NIH-PA Author Manuscript

A. Task-Space Equations of Motion

Let the position on the surface be parameterized by $x \in \mathbb{R}^2$. Define $q:\mathbb{R}^2 \to \mathbb{R}^3$ as the map from the surface parameter to the coordinate corresponding to the point in the Euclidean space, and $p:\mathscr{C} \to \mathbb{R}^3$ as a map from the configuration space to the coordinate of the Euclidean space. The tip of the catheter is in contact with the surface at *x* if the following constraint is satisfied,

$$\phi(\theta, x)=p(\theta) - q(x)=0.$$

For the tip to remain in contact, the following velocity constraint must also be satisfied,

$$\frac{d}{dt}\phi(\theta, x)=\frac{\partial \phi}{\partial \theta}\dot{\theta}+\frac{\partial \phi}{\partial x}\dot{x}=0.$$

Let $J=\partial\phi/\partial\theta \in \mathbb{R}^{3\times 2n}$ and $G^T=-\partial\phi/\partial x \in \mathbb{R}^{3\times 2}$, then the velocity constraint above can be written as

$$J\dot{\theta}=G^T\dot{x}. \quad (6)$$

Because of kinematic redundancy, the joint velocities, denoted by $\dot{\theta}$, cannot be determined uniquely from the task-space velocities, denoted by $\dot{x}$. The joint velocities that lie in the null space of *J* which correspond to $\dot{x}=0$ are called internal motions. Let *H* be a matrix whose rows span the null space of *J*. Then the internal motions can be parameterized by $\upsilon_N=N\dot{\theta}$. Augmenting (6) with the internal motions yeilds

$$\begin{bmatrix} J \\ H \end{bmatrix}\dot{\theta}=\begin{bmatrix} G^T & 0 \\ 0 & I \end{bmatrix}\begin{bmatrix} \dot{x} \\ \upsilon_N \end{bmatrix}.$$

Now, the joint velocities are completely decomposed into the task-space velocity, and the internal motions. Let

$$\overline{J}=\begin{bmatrix} J \\ H \end{bmatrix}, \overline{G}^T=\begin{bmatrix} G^T & 0 \\ 0 & I \end{bmatrix},$$

then $\dot{\theta}$ corresponding to $\dot{x}$ and υ_N can be determined uniquely from

$$\dot{\theta}=\overline{J}^{-1}\overline{G}^T=\begin{bmatrix} \dot{x} \\ \upsilon_N \end{bmatrix}. \quad (7)$$

If *H* is chosen such that its rows are orthonormal among themselves and orthogonal to the rows of *J*, then $\overline{J}^{-1}=[\begin{array}{cc} J^{\dagger} & H^T \end{array}]$, where $J^{\dagger}=J^T(JJ^T)^{-1}$ is the right pseudo-inverse of *J*. Using (3) and (7), the equations of motion of the catheter tip on the surface can be written as

$$\overline{C}(\theta)\begin{bmatrix}\dot{x}\\ \upsilon_N\end{bmatrix}+\overline{N}(\theta)=F \quad (8)$$

where

$$\overline{C}=\overline{GJ}^{-T}C\overline{J}^{-1}\overline{G}^{T},$$
$$\overline{N}=\overline{GJ}^{-T}K\theta,$$
$$F=\overline{GJ}^{-T}\tau,$$

With $\overline{J}^{-T}=(\overline{J}^{-1})^{T}$. We have $\overline{GJ}^{-T}\nabla h(\theta)\lambda=0$, beacuse $\dot{\theta}$ that satisfies (7) do no work on the constraint surface.

Now, the equations of motion are decomposed into tip velocity and internal velocity in (8). Motion planning in the task space is presented next.

B. Motion Planning in the Task Space

First, define the reference trajectory on the surface by a sequence of via points, denoted *X*. The catheter is assumed to be in contact with the surface with some initial configuration θ_0. At this point, the disturbance torques, τ_w, are assumed to be zero as the goal here is to determine the plan in a noise-free environment.

The algorithm starts by moving the tip of the catheter from $p(\theta_0)$ to the first via point in *X*. Then the tip is moved from one via point to the next until every via points is visited.

Define a plan as a pair of discrete-time state and control trajectories (x_k, u_k), $\forall k$. Suppose the tip is at x_k and is moving towards the next via point, denoted by x_g, and the maximum tip velocity is given by $\upsilon \in \mathbb{R}$. The algorithm first determines the desired velocities $\dot{x}^*$ in the gradient direction to x_g, such that $\|\dot{x}\| \le \upsilon$. The task-space velocities are calculated from

$$\dot{x}^*=\begin{cases}\frac{x_g-x_k}{\|x_g-x_k\|}\upsilon, & \text{if}\frac{\|x_g-x_k\|}{\Delta t}>\upsilon\\ \frac{x_g-x_k}{\Delta t}, & \text{if}\frac{\|x_g-x_k\|}{\Delta t}\le\upsilon\end{cases} \quad (10)$$

where Δt is the sampling period. Then (8) is solved with $\dot{x}=\dot{x}^*$ for u^* and υ_N^*. Then $u_k = u^*$ is applied to (3) with zero-order hold for a duration of Δt to obtain x_{k+1}. The algorithm repeats until all the via points are visited.

The pseudo-code of the algorithm is shown in Algorithm 1. The inputs to the planning algorithm are *X* and θ_0, and a trajectory, (x_k, u_k), $\forall k$, is returned by the algorithm.

Algorithm 1 Move the tip of the catheter following via points

1: **procedure** CATHETERMOVE(X, θ_0)

2: $k \leftarrow 1$

3: $\overline{x}_k \leftarrow p(\theta_0), x_g \leftarrow \text{first } x \in X$

repeat
  Determine $\dot{x}^*$ from (10)
  Solve (8), (4), (5) with $\dot{x}=\dot{x}^*$ for u^*
  $u_k \leftarrow u^*$
  Apply u_k to (3) for Δt to obtain x_k
  if Reached(x_{k+1},x_g) **then**
    $x_g \leftarrow$ next $x \in X$
  end if
  $k \leftarrow k + 1$
until All $x \in X$ are visited
return (x_k, u_k), $\forall k$
end procedure

IV. Feedback Policy

The open-loop plan calculated in the previous section is based on the assumption that there are no uncertainties and (3) contains all the information needed to calculate the system trajectory once the control trajectory is determined. In reality, uncertainties, such as, model errors and disturbances are inevitable; hence, a plan that does not take the present states of the system into account will most likely fail. In this paper, disturbances from blood flow is considered. The disturbances are modeled as random forces acting on the catheter.

The catheter is regulated around the open-loop trajectory using a feedback plan calculate using the LQR method [15]. While state feedback is considered in this paper, the formulations can be extended to include a state estimator in the future.

A small-signal model that approximates the behavior of the system in the neighborhood of the trajectory is obtained by linearizing (3) along the trajectory. The small-signal model is then regulated by a finite-time LQR.

A derivations of the small-signal model and the LQR are given in Section IV-A, followed by an application of the feedback control to the catheter in Section IV-B.

A. Small-Signal Model and Linear Quadratic Regulator

The derivation of the LQR around the nominal trajectory is presented in this subsection. First, consider the following control-affine nonlinear system,

$$\dot{x}=f(x)+g(x)u+p(x)w, \quad \text{(11a)}$$

$$y=h(x), \quad \text{(11b)}$$

where x is the state vector, u is the input vector, w is the disturbance vector, and y is the output vector. A discrete-time system can be obtained from the nonlinear system from the following approximation,

$$x_{k+1} \approx x_k+\Delta t(f(x_k)+g(x_k)u_k+p(x_k)w_k),$$
$$y_k=h(x_k).$$

Suppose the system is to be regulated around a trajectory $(x,u,y)=(\overline{x},\overline{u},\overline{y})$, which is calculated assuming $w = 0$. A small-signal system that is valid in the neighborhood of the trajectory can be obtained by linearizing the nonlinear system around the trajectory. Let the small variations from the nominal trajectory be denoted by $\tilde{x}=x-\overline{x}$, $\tilde{u}=u-\overline{u}$, and $\tilde{y}-y-\overline{y}$. The small-signal system is then given by,

$$\tilde{x}_{k+1} \approx F_k\tilde{x}_k+G_k\tilde{u}_k+P_kw_k, \quad \text{(12a)}$$

$$\tilde{y}_k \approx H_k\tilde{x}_k. \quad \text{(12b)}$$

where

$$F_k=I+\Delta t\tfrac{\partial f}{\partial x}(\overline{x}_k)+\Delta t\sum_{\forall i}\frac{\partial g_i}{\partial x}(\overline{x}_k)\overline{u}_i,$$
$$G_k=\Delta t\, g(\overline{x}_k), P_k=\Delta t\, p(\overline{x}_k), H_k=\tfrac{\partial h}{\partial x}(\overline{x}_k).$$

Let the performance measure of the system be the sum of quadratic functions of $\tilde{y}$ and $\tilde{u}$,

$$J(\tilde{x},\tilde{u})=\sum_{k=2}^{N}(\tilde{y}_k^TQ_k\tilde{y}_k+\tilde{u}_{k-1}^TR_k\tilde{u}_{k-1}) \quad \text{(13a)}$$

$$=\sum_{k=2}^{N}(\tilde{x}_k^TH_k^TQ_kH_k\tilde{x}_k+\tilde{u}_{k-1}^TR_k\tilde{u}_{k-1}). \quad \text{(13b)}$$

The small-signal control $\tilde{u}$ is obtained by minimizing (13) of the system described by (12).

$$\underset{\tilde{u}}{\text{minimize}} \;\; J(\tilde{x},\tilde{u}) \quad \text{(14a)}$$

$$\text{subject to} \;\; \tilde{x}_{k+1}=F_k\tilde{x}_k+G_k\tilde{u}_k+P_kw_k, \quad \text{(14b)}$$

$$\tilde{y}_k=H_k\tilde{x}_k. \quad \text{(14c)}$$

The optimal solution of (14) is a linear state-feedback control law of the form

$$\tilde{u}_k=L_k\tilde{x}_k. \quad \text{(15)}$$

The variable feedback gain, L_k, is calculated backward recursively as

$$L_k=-\left(G_k^TS_{k+1}G_k+R_k\right)^{-1}G_k^TS_{k+1}F_k, \quad \text{(16a)}$$

$$S_k = H_k^T Q_k H_k + F_k^T S_{k+1} F_k + F_k^T S_{k+1} G_k L_k, \quad (16b)$$

with the boundary condition $S_N = H_N^T Q_N H_N$ [15].

B. Feedback Policy of the Catheter

The LQR feedback controller developed in the previous section is used to regulate the position of the tip on the surface, *x*, around the open-loop trajectory, $\overline{x}$. Since τ_u and τ_w are linear in *u* and *w* respectively, the following control-affine system in (11) can be obtained from (3),

$$\dot{\theta} = -C(\theta)^{-1} K\theta - C(\theta)^{-1} \nabla h(\theta)\lambda + C(\theta)^{-1}\tau, \quad (17a)$$

$$x = q^{-1}(p(\theta)), \quad (17b)$$

where *p* and *q* are defined in Section III, and τ is affine in *u* as defined in (4) and (5). The system is discretized to obtain a discrete-time small-signal model as in (12). Then the feedback control law, $\tilde{u}_k = L_k \tilde{\theta}_k$, is calculated by solving (16) from $k = N$ to $k = 1$.

V. Simulation Results

A 3-link catheter model with the coils attached to the second link is considered in the simulations. The first two links from the base of the catheter represent the deflection that is controllable by the actuator, while the last link represents the deflection that cannot be controlled directly. External forces acting of the catheter is assumed to be a lumped force acting on the second link. The parameters used in the simulations are listed in Table I.

Four simulations are presented. Two straight-line trajectories are considered in Section V-A. These simulations demonstrate the catheter's ability to move along two orthogonal directions on the surface. Two simulations of the catheter performing ablation are studied in Section V-B. A simulation in a noise-free environment is presented first followed by a simulation that includes Brownian motion disturbances.

A. Straight-Line Trajectories

The simulation results in this section demonstrate the catheter's ability to move its tip on a surface along two orthogonal directions which are aligned with the *x*- and *y*-axis of the catheter's base frame for simplicity. The base frame is, in turn, aligned such that the MR magnetic field is orthogonal to the *x*-axis.

The movement of the catheter along the two orthogonal directions are shown in Fig. 2, and the currents that move the catheter along the two trajectories are shown in Fig. 3, respectively. The currents required to move the tip along the *x* direction are higher, as shown in the Fig. 3a, because the magnetic field in that direction is zero, so only the *z* component of the magnetic field is available for creating the required joint torques. The catheter also slightly bends side way along the way as can be seen in Fig. 2a.

The magnetic moments calculated by the algorithm are perpendicular to the magnetic field which results in minimal control effort needed. This is clearly demonstrated by the movement along the *y*-axis case where the catheter remain aligned with the *y*-axis (Fig. 2b) and the *x*-axis coil, which remains orthogonal to the magnetic field during the simulation, is not activated (Fig. 3b).

B. Circular Trajectory

The simulation in this section is modeled after a catheter ablation procedure where the catheter enters the left atrium from the right atrium and creates a circular lesion around the pulmonary veins. The procedure and its approximation are illustrated in Fig. 4.

First, a sequence of 100 via points, denoted by X, is sampled from a counter-clockwise circular trajectory with the radius of 12 mm. Then an open-loop plan is calculated using Algorithm 1 with the sequence of via points and an initial catheter configuration as inputs. The open-loop trajectory of the tip and the movement of the catheter are shown in Fig. 5. The input current is shown in Fig. 6. Note that the currents become discontinuous when a new via point is selected as the target. This can be remedied by slowly varying the direction of the catheter’s tip from one via point to the next.

Then, a feedback policy is calculated using the method in Section IV. A sampling-time of 1 second is used for the feedback controller to reflect the fact that the frame rate of MRI is around 5 frames per second [4], [5], and multiple images are needed to estimate the configuration of the catheter.

Twenty simulations with Brownian motion disturbances are shown in Fig. 7. The trajectories with feedback policy stay much closer to the desired trajectory while the open-loop trajectories do not resemble the circular path ten out of the twenty trials.

VI. Conclusion

This paper presents a motion-planning algorithm of MRI-actuated catheters for catheter ablation of atrial fibrillation. The catheter is modeled as an n-link manipulator with elastic spherical joints. Due to high degrees of freedom of the catheter model relative to the task space and actuation, the catheter suffers from kinematic redundancy and underactuation. The difficulties are circumvented by performing motion planning in the task space instead of the configuration space. The algorithm first calculates an open-loop plan that moves the tip of the catheter following a predefined trajectory in a disturbance-free environment. A small-signal model of the system operating around the open-loop trajectory is obtained by linearization. An LQR for the small-signal model is then added to the existing open-loop plan to enhance the system’s robustness to disturbances. The efficacy of the planning algorithm is demonstrated by Matlab simulations.

While the catheter in this paper has one set of coils, adding additional coils leads to higher actuation degrees of freedom, which would allow other performance measures besides tip movement to be considered in motion planning. Selecting the transseptal puncture and initial contact configuration is another interesting area since they directly affect motion planning.

Other perturbations such as heart motion and model error have not been studied in this paper but they will be included in the future works. Measurement feedback control and active sensing via MRI images is also a part of the future work.

Acknowledgments

This work was supported in part by NSF under grants IIS-0905344 and CNS-1035602, and National Institutes of Health under grants R21 HL096941 and R01 EB018108.

References

1. Calkins H, Kuck KH, Cappato R, Brugada J, Camm AJ, et al. 2012 hrs/ehra/ecas Expert Consensus Statement on Catheter and Surgical Ablation of Atrial Fibrillation: Recommendations for Patient Selection, Procedural Techniques, Patient Management and Follow-up, Definitions, Endpoints, and Research Trial Design. Europace. Apr; 2012 14(4):528–606. [PubMed: 22389422]
2. Cappato R, Calkins H, Chen S-A, Davies W, Iesaka Y, et al. Updated Worldwide Survey on the Methods, Efficacy, and Safety of Catheter Ablation for Human Atrial Fibrillation. Circulation: Arrhythmia and Electrophysiology. Feb; 2010 3(1):32–38. [PubMed: 19995881]
3. Chun KRJ, Schmidt B, Köktürk B, Tilz R, Fürnkranz A, et al. Catheter Ablation New Developments in Robotics. Herz. Dec; 2008 33(8):586–589. [PubMed: 19137249]
4. Nazarian S, Kolandaivelu A, Zviman MM, Meininger GR, Kato R, et al. Feasibility of Real-Time Magnetic Resonance Imaging for Catheter Guidance in Electrophysiology Studies. Circulation. Jul; 2008 118(3):223–229. [PubMed: 18574048]
5. Vergara GR, Vijayakumar S, Kholmovski EG, Blauer JJE, Guttman MA, et al. Real-time magnetic resonance imagingguided radiofrequency atrial ablation and visualization of lesion formation at 3 Tesla. Heart Rhythm. Feb; 2011 8(2):295–303. [PubMed: 21034854]
6. Gudino N, Heilman JA, Derakhshan JJ, Sunshine JL, Duerk JL, et al. Control of intravascular catheters using an array of active steering coils. Medical Physics. 2011; 38(7):4215–4224. [PubMed: 21859023]
7. Roberts TPL, Hassenzahl WV, Hetts SW, Arenson RL. Remote control of catheter tip deflection: An opportunity for interventional MRI. Magnetic Resonance in Medicine. Dec; 2002 48(6):1091–1095. [PubMed: 12465124]
8. Khoshnam, M.; Azizian, M.; Patel, RV. Robotics and Automation (ICRA), 2012 IEEE International Conference on. IEEE; May. 2012 Modeling of a steerable catheter based on beam theory; p. 4681-4686.
9. Liu, T.; Cavusoglu, MC. Robotics and Automation (ICRA), 2014 IEEE International Conference on. IEEE; Three Dimensional Modeling of an MRI Actuated Steerable Catheter System. to be published
10. Khoshnam, M.; Patel, RV. Robotics and Automation (ICRA), 2013 IEEE International Conference on. IEEE; May. 2013 A pseudo-rigid-body 3R model for a steerable ablation catheter; p. 4427-4432.
11. Penning, RS.; Jung, J.; Ferrier, NJ.; Zinn, MR. Robotics and Automation (ICRA) 2012 IEEE International Conference on. IEEE; May. 2012 An evaluation of closed-loop control options for continuum manipulators; p. 5392-5397.
12. Conrad BL, Jung J, Penning RS, Zinn MR. Interleaved continuum-rigid manipulation: An augmented approach for robotic minimally-invasive flexible catheter-based procedures. Robotics and Automation (ICRA) 2013 IEEE International Conference on IEEE. May.2013 :718–724.
13. Xu R, Asadian A, Naidu AS, Patel RV. Position control of concentric-tube continuum robots using a modified Jacobian-based approach. Robotics and Automation (ICRA) 2013 IEEE International Conference on IEEE. May.2013 :5813–5818.
14. Murray, RM.; Li, Z.; Sastry, SS.; Sastry, SS. A Mathematical Introduction to Robotic Manipulation. 1. CRC Press; Mar. 1994
15. Anderson, BDO.; Moore, JB. Optimal Control: Linear Quadratic Methods. Prentice Hall; 1990. Prentice Hall Information and System Sciences Series

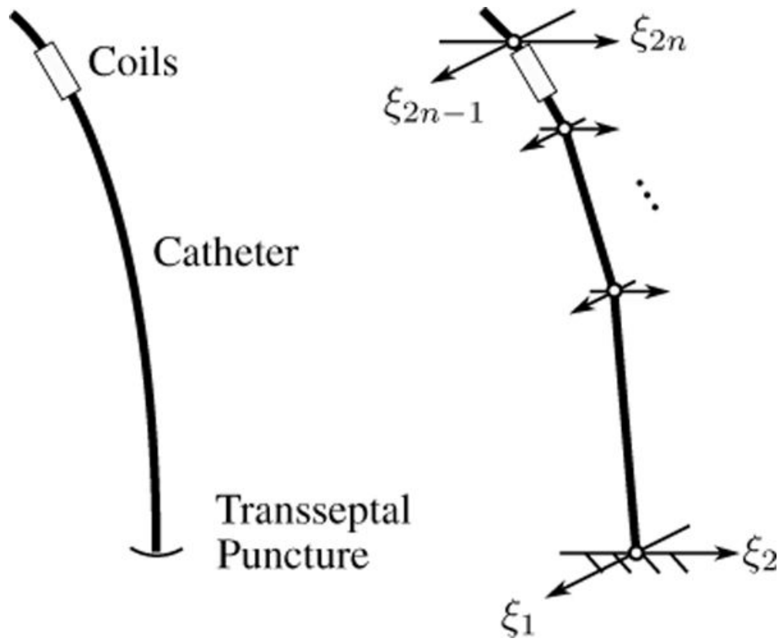

Fig. 1.

On the left is the catheter as a continuum manipulator. The coils attached generates magnetic moments, $u \in \mathbb{R}^3$, which is used to steer the catheter under MR magnetic field. A *n*-link approximated model of the catheter is depicted on the right ($n = 4$ in this case). The continuous catheter body is discretized into *n* rigid links connected by passive spherical joints. The elasticity of the catheter is captured by the torsional springs located at the joints. The catheter is equipped with one set of orthogonal coils. The twists of the manipulator are denoted by ξ_i, $i = 1,\ldots,2n$.

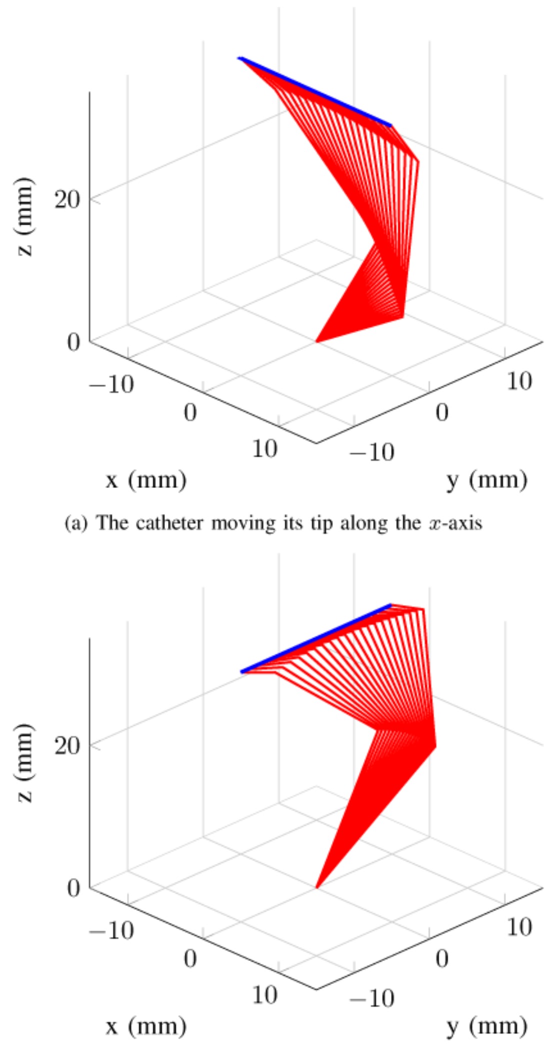

(a) The catheter moving its tip along the x-axis

(b) The catheter moving its tip along the y-axis

Fig. 2.

The catheter moving its tip along two orthogonal directions on the surface. The blue lines are the tip trajectories and the body of the catheter is shown in red.

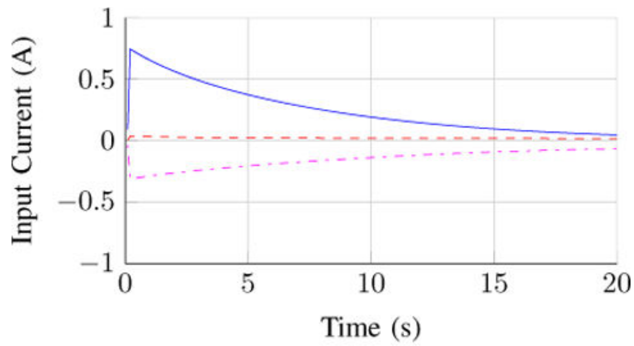

(a) The current that moves the tip along the x-axis

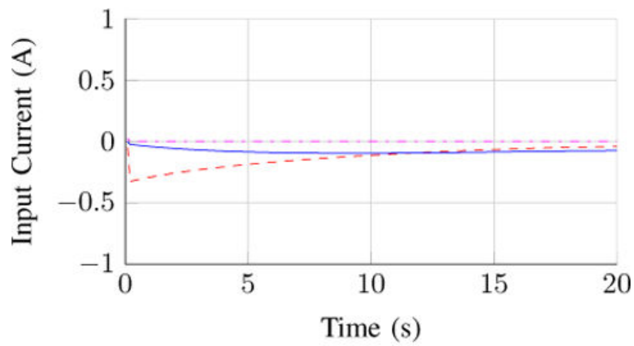

(b) The current that moves the tip along the y-axis

Fig. 3.

The input currents as a function of time. The dash-dot magenta line, the dash red line, and the solid blue line, correspond to the *x*-, *y*-, and *z*-axis aligned coil respectively.

NIH-PA Author Manuscript
NIH-PA Author Manuscript

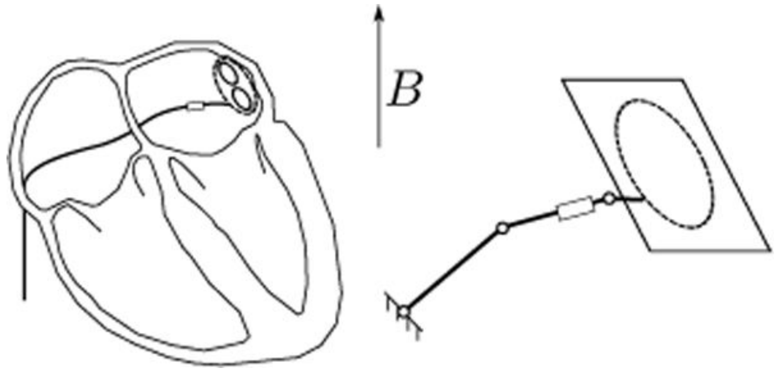

Fig. 4.
The catheter performing ablation of atrial fibrillation in the left atrium. The configuration of the surface and MR magnetic field with respected to the catheter are depicted on the right.

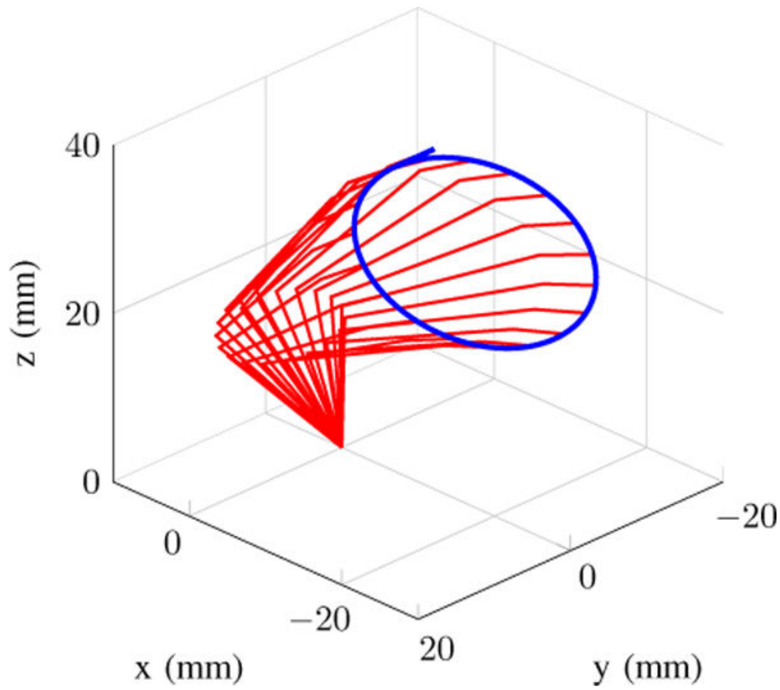

Fig. 5.
The catheter moving the tip along a circular trajectory on the surface.

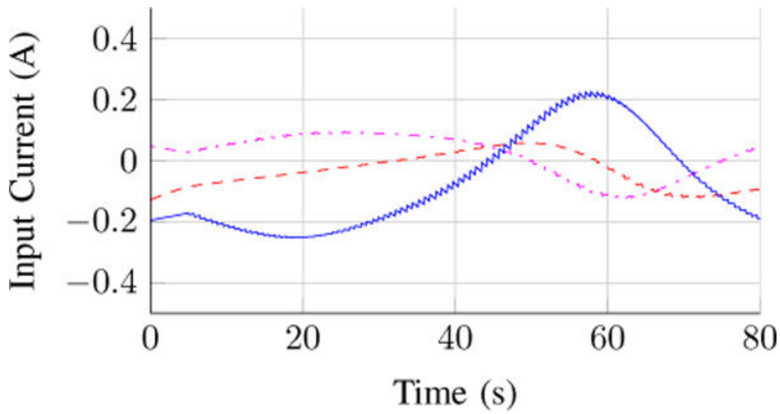

Fig. 6.

The input current used to move the tip of the catheter along the circular trajectory. The dash-dot magenta line, the dash red line, and the solid blue line, correspond to the *x*-, *y*-, and *z*-axis aligned coil respectively.

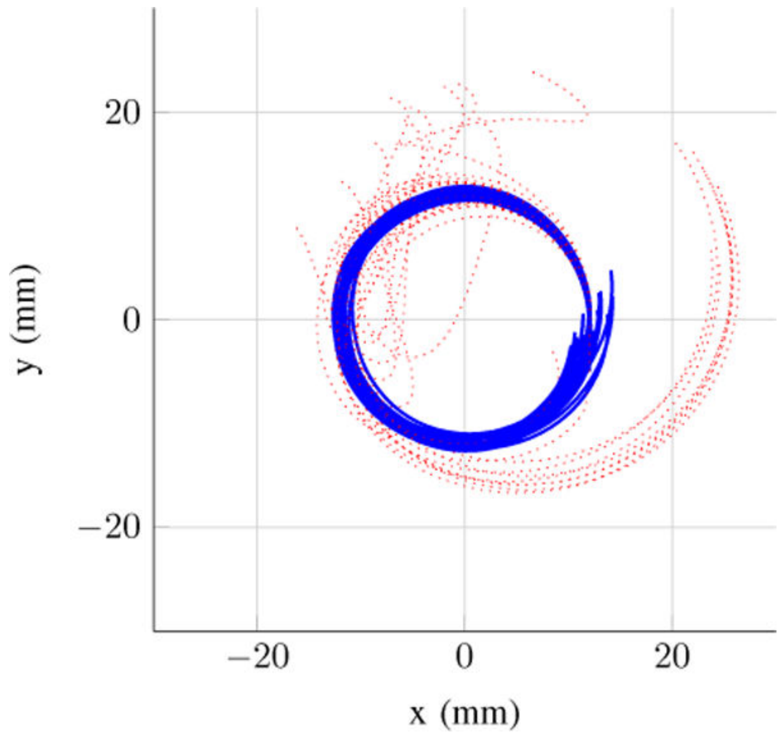

Fig. 7.

Twenty trials of the simulation with Brownian motion disturbances are shown in this figure. The solid lines are the trajectories of the catheter's tip with feedback control while the dotted lines are the trajectories without feedback control. Note that the feedback reduces the variability of the trajectories significantly and ten out of twenty trails of the open-loop trajectories do not resemble the desired circular trajectory.

TABLE I

Simulation parameters

Parameter	Value
Viscous damping coefficient (N-m-s)	diag(5,5,5,5,1.25,1.25) $\times 10^{-5}$
Spring stiffness coefficient (N-m)	diag(6,6,6,6,6,6) $\times 10^{-6}$
Disturbances step size	$[-1 \times 10^{-5}, 1 \times 10^{-5}]$
Length of link 1, 2 and 3 (mm)	20, 20 and 10
Magnetic field, (T)	$\left[0 - 1.5/\sqrt{2}\, 1.5/\sqrt{2}\right]^T$
Surface origin (Section V-A) (mm)	$[0\ 0\ 35]^T$
Surface normal (Section V-A), n_0	$[0\ 0\ 1]^T$
Surface origin (Section V-B) (mm)	$[-17.5\ 0\ 30.3]^T$
Surface normal (Section V-B), n_0	$\left[-1/20\ \sqrt{(3)}/2\right]^T$
Axial and side coils dimension (mm^2)	$\pi(0.5)^2$, 2×4
Axial and side coils number of turns	70, 15
Nominal tip velocity, (mm/s)	1.0
Sampling-time (s)	0.1
Feedback control sampling-time (s)	1.0
Friction coefficient	0.1